



Article

Novel Method for NTC Thermistor Production by Aerosol Co-Deposition and Combined Sintering

Michaela Schubert ¹, Christian Münch ², Sophie Schuurman ³, Véronique Poulain ³, Jaroslaw Kita ¹  and Ralf Moos ^{1,*} 

¹ Department of Functional Materials, Universität Bayreuth, 95440 Bayreuth, Germany; functional.materials@uni-bayreuth.de

² Vishay Electronic GmbH, Dr.-Felix-Zandman-Platz 1, 95100 Selb, Germany; CC-NLR-Division@vishay.com

³ Vishay Resistors Belgium BVBA, Twee Huizenstraat 37, 1140 Brussel, Evere, Belgium; CC-NLR-Division@vishay.com

* Correspondence: functional.materials@uni-bayreuth.de; Tel.: +49-(0)921-55-7401

Received: 19 March 2019; Accepted: 1 April 2019; Published: 5 April 2019



Abstract: A novel three-stage process to produce NTCR sensors is presented. In this process, an uncalcined powder mixture of NiO and Mn₂O₃ was deposited onto an alumina substrate via aerosol co-deposition (AcD). Then, an electrode structure was screen-printed onto the surface and the composite film was sintered in a multifunctional temperature treatment. Thereby, the sintering of the electrode, the formation of the NiMn₂O₄ spinel and the removal of film strains took place simultaneously. This enabled a significant reduction in energy demand and workload. The manufactured sensors, both as first prototypes, as well as miniaturized chip components, were characterized by a single-phase cubic NiMn₂O₄ spinel structure, mechanical stability and electrical properties that were similar to those of classical NiMn₂O₄ bulk ceramics or tempered aerosol deposited (AD) NiMn₂O₄ films. Particularly noteworthy was the high reproducibility and low variation of the NTCR parameters, such as the specific resistivity at 25 °C ρ_{25} , the electrical resistance at 25 °C R_{25} and the thermistor constant B . The NTCR parameters were as aging-stable as for NiMn₂O₄ bulk ceramics or tempered NiMn₂O₄ AD-films and could even be further improved by thermal post-treatment.

Keywords: aerosol deposition method (ADM), RTIC; NiMn₂O₄ ceramic; NTCR device; temperature sensor; thick film thermistor

1. Introduction

Due to their high-temperature sensitivity, reliability, and low-cost, ceramic NTC thermistors are widely used as temperature sensors in industrial, domestic and medical applications [1–4]. They are mainly based on transition metal spinel manganites ($0 < x < 1$, M: Ni, Co, Cu, etc.) [5,6], such as NiMn₂O₄, and are characterized by an almost exponential drop in electrical resistance with increasing temperature. The operating temperature of spinel-based NTC thermistors is in the range of -50 °C to 150 °C [7]. The high-temperature dependence of the electrical resistance R is based on a small polaron hopping, a conduction mechanism based on phonon-assisted hopping of charge carriers along Mn³⁺ and Mn⁴⁺ cations on octahedral interstices, via localized states [6,8]. The R - T -behavior can be described by the Arrhenius equation [9–11]:

$$R(T) = R_0 \cdot \exp(E_A / (k_B \cdot T)) = R_0 \cdot \exp(B/T) \quad (1)$$

where R_0 is the electrical resistance at infinitely high temperature and T is the temperature in Kelvin. The quotient of the activation energy for the hopping process E_A and the Boltzmann constant k_B is

defined as the so-called B constant. Besides the resistivity at 25 °C ρ_{25} , this is an important parameter to describe and compare NTCR ceramics. The commercial production of NTCR ceramic sensors is based almost exclusively on traditional, sinter-based processes [5,12]. In these processes, a pre-calcined (600 °C to 800 °C) ceramic powder is usually formed by processes such as pressing, extrusion, film casting, and eventually sintered at temperatures above 1000 °C under controlled atmospheres [2,12]. However, the thermistors produced with these processes are limited in terms of their integration capability in electronic circuit boards and miniaturization [7]. Therefore, different thin and thick film processes for the production of ceramic NTCR sensors are currently being investigated [7]. The aerosol deposition (AD) process has proven to be extremely promising. Starting from ceramic powder, dense ceramic films can be produced at room temperature and on a wide variety of substrate materials [13–16]. The films are characterized by a high density, good substrate adhesion as well as a nanocrystalline film structure and production-related film strains. Even NTC thermistors can be deposited directly from the spinel-based ceramic powder at room temperature [17–21]. The NTCR films are mechanically stable and exhibit NTCR parameters (ρ_{25} , B), which are only slightly above those of the classic bulk ceramics, as found in References [4,5,22,23]. By a mild tempering (60 minutes at 400 °C) the NTCR parameters can even be varied slightly and reach the bulk values [19].

Despite the excellent thermistor properties, the process as it is described in References [18,19,24] has the disadvantage of the many process steps. As described above, a complete spinel formation is necessary, which requires a multi-stage powder preparation. It involves a combined powder mixing and milling, drying and calcining at 900 °C, followed by a second powder milling, drying and sieving. In addition, electrodes must be applied separately to the substrate, e.g., by screen-printing and subsequent electrode firing at 700 °C to 900 °C. In order to achieve thermally stable properties comparable to those of bulk ceramics, it is necessary to heat treat the produced films again to reduce film strains, increase grain size and reduce the number of grain boundaries.

A way to simplify the process is the novel method described in this paper. It combines the already known method of aerosol co-deposition (AcD), which is the deposition of a ceramic powder mixture, as described in References [25–27], with a multifunctional sintering step, in which the composite film is in situ calcined, tempered, and the screen-printed electrodes are sintered simultaneously. This process not only eliminates the second milling and drying step, but also combines the previous three temperature treatments (powder calcination, electrode firing, film tempering) into one thermal process step.

In the first part of this study, the feasibility of the process is presented on the basis of first demonstrator devices, as well as accompanying XRD measurements, SEM analyses and electrical measurements. The second part of this study shows the implementation of the concept into chip-based NTC thermistor components of the size 3.2 mm × 1.6 mm (size 1206). Likewise, electrical measurements and aging tests were carried out.

2. Materials and Methods

The initial step is the powder mixing. The raw materials, preparation equipment and preparation route are described in detail by Schubert et al. [27]. The finished powder mixture is analyzed via XRD (D8 ADVANCE, Bruker AXS, Bruker Corporation, Billerica, USA). Afterward, the first prototypes were manufactured in three steps according to the new method (see Figure 1). In the first step, as shown in Figure 1a, the aerosol co-deposition on a bare alumina substrate (Rubalit 710, CeramTec) took place. The apparatus used for the deposition process is described in detail by Hanft et al. [28]. The apparatus basically consisted of a vacuum pump, a deposition chamber and an aerosol-generating unit (here, a fluidized bed). During the process, the carrier gas oxygen with a flow rate of 6 l/min was forced through a loose filling of the powder mixture and thus an aerosol was generated. A pressure difference between the aerosol generation unit (~20 kPa) and the deposition chamber (~0.5 kPa) caused the powder aerosol to be transported into the deposition chamber. The powder aerosol passed the nozzle (0.5 × 10 mm slot nozzle) and was further accelerated to several hundred meters per second.

In the deposition chamber (schematically shown in Figure 1a), suitable particles of NiO and α -Mn₂O₃ collided with the alumina substrate. The substrate was placed at a distance of 4–5 mm from the nozzle and was moved at a speed of 1 mm/s, perpendicular to the nozzle. On impact with the substrate, the particles deformed and/or broke up into fragments in the nanometer range. The particle fragments bonded onto each other and onto the substrate. By this deposition mechanism, they formed a firmly adherent ceramic composite film of NiO and α -Mn₂O₃ under the influence of other impacting particles (densification was by the hammering effect, Room Temperature Impact Consolidation (RTIC) mechanism [13]).

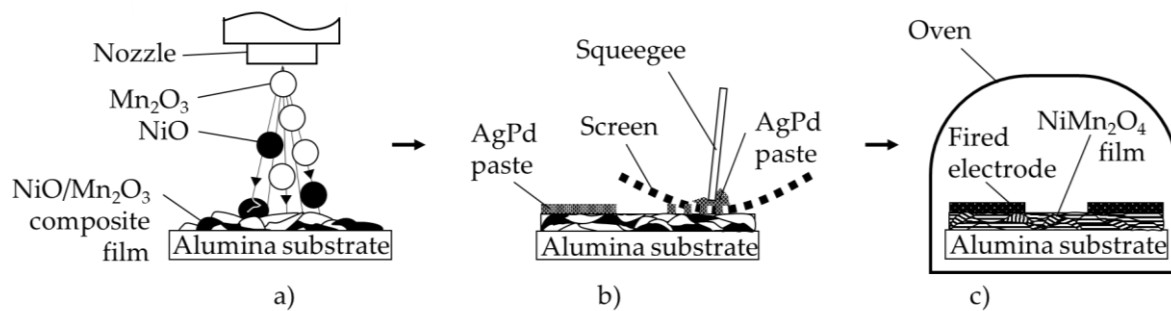


Figure 1. Scheme of the novel NTC thermistor production route, (a) aerosol co-deposition (AcD) of the powder mixture of NiO and Mn₂O₃; (b) application of an electrode structure by screen-printing; (c) combined electrode sintering with spinel formation and film tempering.

In the second step of the method (Figure 1b), an interdigital electrode structure (29 electrode finger pairs, finger length 4.7 mm, line/space 100 μ m) was screen-printed onto the surface of the composite film using an AgPd paste (6146, DuPont). In the third and last step, the films were heated to 850 $^{\circ}$ C for 10 min. In this step, the screen-printed electrode was fired, and simultaneously, the composite film was calcined and tempered. In order to investigate the influence of the deposition process and the temperature treatment on the crystal structure, XRD analyses (PANalytical XPert Pro, PANalytical, Almelo, Netherlands) were performed in parallel to sensor manufacturing. For this purpose, the powder mixture was co-deposited under identical parameters onto a Si-wafer. The film was examined in the deposited state and in the in situ calcined state at room temperature. In addition, the spectra were evaluated with regard to the strain ε and the crystallite size L using the Williamson–Hall method:

$$\Delta(2\Theta) \cdot \cos(\Theta) = (K \cdot \lambda) / (L) + 4 \cdot \varepsilon \cdot \sin(\Theta) \quad (2)$$

where K is the dimensionless Scherrer constant ($K = 0.9$), λ is the wavelength of the X-ray source (here Cu $K\alpha_1$: 1.5406 \AA) and Θ is the Bragg angle. The reflex broadening in half of the maximum $\Delta(2\Theta)$ was determined via the Lorentz fit function. The prepared sensors were characterized by SEM (Leo 1450 VP, Zeiss, Oberkochen, Germany). Electrical resistance measurements were carried out (four-wire setup) in the in situ calcined state and in the aged state, in a thermostat bath (Julabo SL-12, Julabo GmbH, Seelbach, Germany) with low viscosity silicone oil (dow corning 200 fluid, 5 cst., Dow Corning Corporation, Midland, MI, USA) using a digital multimeter (Keithley 2700, Keithley Instruments Inc., Solon, OH, USA). The bath temperature was controlled by a precision Pt1000 device. The aging of the sensors took place at 125 $^{\circ}$ C for 1000 h under air.

In order to apply the novel three-stage process (see Figure 1) for chip-based components, an AcD was performed on a laser-patterned (breaking edge) alumina substrate (Rubalit 710, CeramTec). In the second step (Figure 1b), an interdigital electrode structure (9 electrode finger pairs, finger length 2.13 mm) was applied onto the composite film by the screen-printing of an Au paste (5744R, DuPont). The distance between the electrode fingers and the finger width was 70 μ m each. In the third step (Figure 1c), the multifunctional temperature treatment took place at 850 $^{\circ}$ C for 10 min. Finally,

the components were separated manually. The components were electrically characterized in the in situ calcined state and in the aged state. The electrical measurement was carried out in a silicone oil bath (same set up as above) at 25 °C and 85 °C. The devices were aged for 1000 h at 125 °C after the in situ calcination and after an additional pre-treatment step at 600 °C for 60 min.

3. Results and Discussion

3.1. Characterization of the First Prototypes

Figure 2 shows an NTCR sensor after completion of the multifunctional temperature treatment. The combination of the alumina substrate, the aerosol deposited film, and the screen-printed AgPd interdigital electrode was mechanically stable. No cracks, spalling or delamination were visible. Both the electrode and the aerosol deposited NTCR film did neither peel off in the tape test nor by mechanical scratching. The electrode structure was precisely deposited and showed no short-circuits.

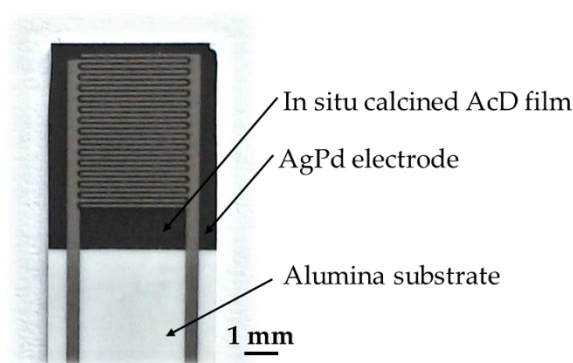


Figure 2. Finished NTCR sensor after completion of multifunctional temperature treatment.

Good adhesion of the film to the substrate and to the electrode was also confirmed in the SEM analysis of the fracture surface (see Figure 3). In the lower part of the SEM image is the alumina substrate, in the middle is the AcD film, and at the upper end is the AgPd electrode. No cracks or delamination could be detected within the NTCR sensor. The adhesion of both the AcD film on the substrate and the AgPd electrode on the AcD film was very good after in situ calcination. The AgPd film has the typical structure of screen-printed films consisting of sintered metal beads. Compared to the screen-printed AgPd film, the in situ calcined AcD film was very dense. However, the calcined AcD film morphology differed noticeably from classic AD films in the as-deposited state [18,19]. Thus, in the lower half of the film, AD untypical pores in the range of 10 nm to 100 nm occurred. The upper half of the film showed a recrystallized structure of uniform, octahedral grains in the range of 100 nm, similar to grains produced via an oxalic precursor route [5].

The pores formed in the lower half of the film were due to grain growth and the release of oxygen. Oxygen was released during the intermediate reaction $\text{NiMnO}_3 + 1/2 \alpha\text{-Mn}_2\text{O}_3 \rightarrow \text{NiMn}_2\text{O}_4 + 1/4 \text{O}_2$ [23,29], and could not diffuse outwards due to the high film density. The recrystallization in the upper half of the film may have been due to sintering additives from the screen-printing paste. However, diffusion of Ag, Pd or other elements into the film could not be detected by energy dispersive X-ray (EDX).

The results of the accompanying XRD analysis are shown in Figure 4. Figure 4a shows the XRD spectrum of the initial powder mixture of NiO and Mn₂O₃, Figure 4b shows the spectrum of the AcD film in the as-deposited state and Figure 4c shows the spectrum of the AcD film after the in situ calcination. The analysis of the three spectra (Figure 4a–c) using the Williamson–Hall method is shown in Figure 4d. It is shown that only reflections of cubic NiO (PDF-Nr. 01-073-1523) and cubic $\alpha\text{-Mn}_2\text{O}_3$ (PDF-Nr. 01-078-0390) could be found, both in the powder mixture (Figure 4a) and in the AcD film in the as-deposited state (Figure 4b). Consequently, during the powder production and

co-deposition process, there was no change in the crystal structure compared to the starting oxides. The reflexes in the AcD film (Figure 4b) were very strongly widened with low intensity. This is typical for AD films and was due to the nanocrystalline film structure and the film strains caused by the RTC mechanism [30–32]. The evaluation of the strain and crystallite size using the Williamson–Hall method (see Figure 4d) gave a strain of about 0.5% and crystallite sizes of about 30 nm for NiO, and about 1% and 29 nm for Mn_2O_3 .

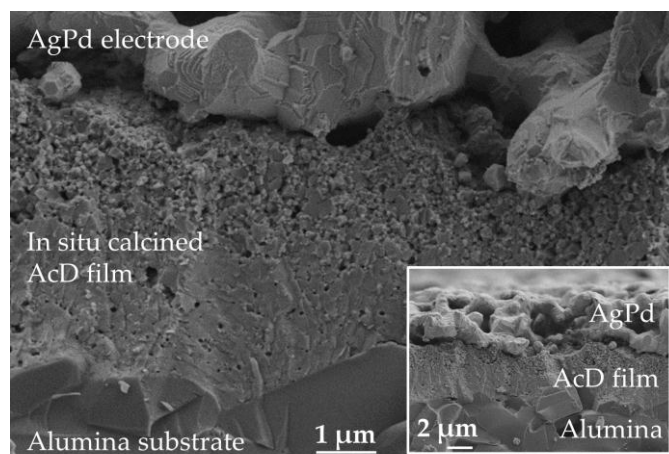


Figure 3. SEM analysis of the fracture surface after calcination of the sensor.

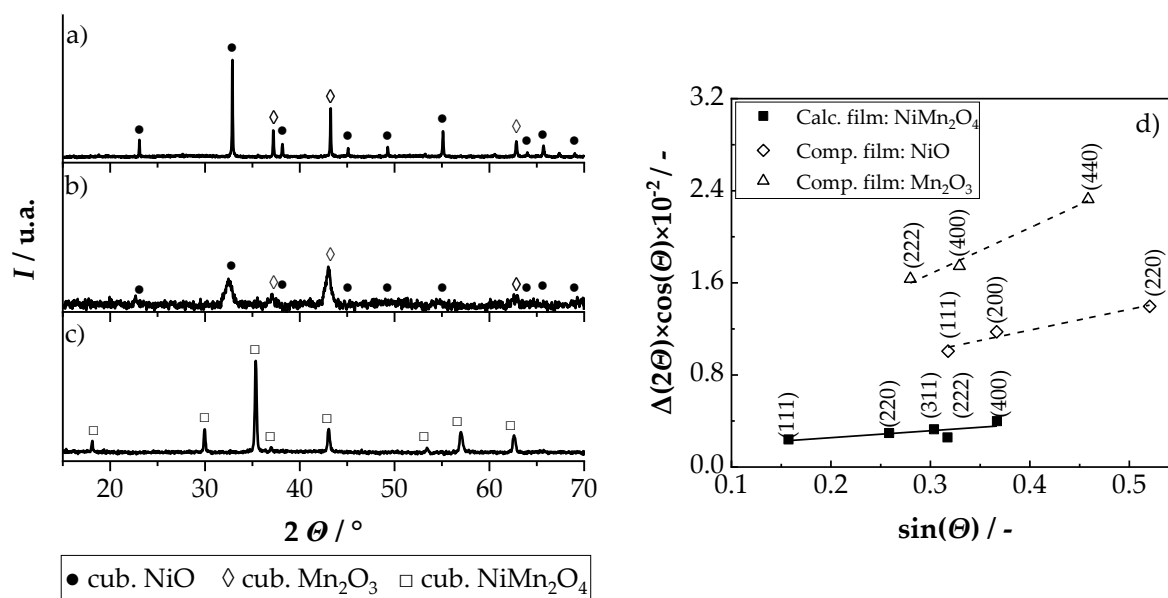


Figure 4. XRD spectra of (a) starting powders, (b) AcD film in the as-deposited state, (c) AcD film after calcination and (d) Williamson–Hall plots of NiO and $\alpha\text{-Mn}_2\text{O}_3$ in composite film in the as-deposited states and NiMn_2O_4 after calcination of the composite film; (NiO: PDF-Nr. 01-073-1523; $\alpha\text{-Mn}_2\text{O}_3$: PDF-Nr. 01-078-0390; NiMn_2O_4 : PDF-Nr. 01-084-0542).

This high strain and the very small crystallite size were consistent with the literature [30,33–36]. After the in situ calcination (Figure 4c), the XRD spectrum showed only the reflexes of a cubic NiMn_2O_4 (PDF-Nr. 01-084-0542) spinel. Thus, it could be proved that an in situ calcination of an AcD film to the desired NiMn_2O_4 is possible. Also, the reflexes were significantly narrower and with more intensity compared to the deposited state. As a result, internal film strains could be reduced during calcination and the crystallite size could be increased. This was also confirmed by an evaluation of the spectrum

using the Williamson–Hall method (Figure 4d), which showed a crystallite size of 103 nm and a strain of only 0.1%.

The single-phase cubic NiMn_2O_4 spinel structure and the almost completely eliminated film strains were also reflected in the NTCR characteristic achieved. Thus, the manufactured components, as demonstrated on the example of sensors 1 and 2 (Figure 5a), exhibited the typical exponential NTCR behavior. With a room temperature resistance R_{25} in the range of 10 k Ω , the sensors were in a range that was appropriate for typical applications. Particularly noteworthy, were the achieved NTCR parameters ρ_{25} and B in Figure 5b. With 25.5 $\Omega\text{ m}$ and 3825 K, the parameters were exactly in the range of those of classic NiMn_2O_4 bulk ceramics ($B = 3500\text{ K} - 3900\text{ K}$, $\rho_{25} = 20\text{ }\Omega\text{ m} - 30\text{ }\Omega\text{ m}$ [4,5,22,23]). This is a major advantage of the process compared to conventional AD process, in which an additional tempering step is required to reduce film strains, increase grain size and reduce the number of grain boundaries in order to achieve the bulk characteristics [17–19].

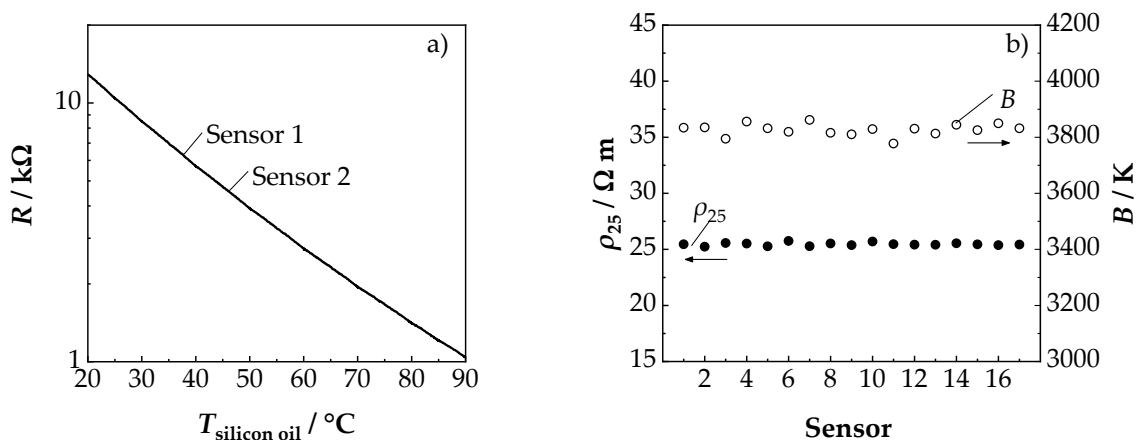


Figure 5. (a) R - T characteristics of two randomly chosen sensors (number 1 and 2 from Figure 5b) and (b) determined B and ρ_{25} values of all 17 produced sensors.

Another positive aspect was the very good reproducibility of the NTCR parameters ρ_{25} and B . As shown in Figure 5b, both the ρ_{25} and the B value of the 17 sensors scattered below $\pm 1\%$ around the average value. This proved the good reproducibility of the suggested novel device preparation method. The aging results of the sensors for 1000 h at 125°C are shown in Figure 6. It could be seen that the main change of B and ρ_{25} and occurred within the first 100 h. This is typical for NTCR ceramics and has been frequently observed in the literature [5,37,38].

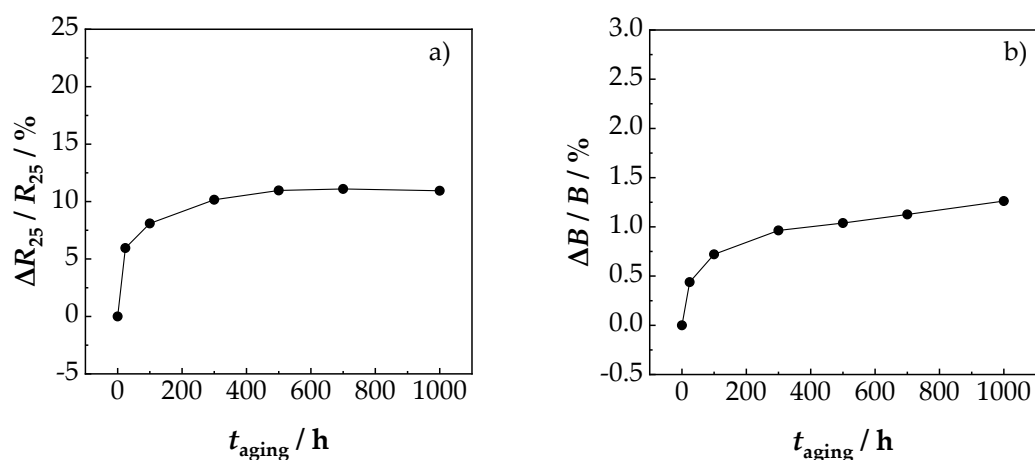


Figure 6. Influence of aging for 1000 h at 125°C on (a) R_{25} value and (b) B value.

After aging for 1000 h at 125 °C, the B value changed by about 1%, and the R_{25} value by about 11%. Thus, the resistance increase rate due to aging was in the range of classical bulk NiMn_2O_4 sensors (10%–15% [5,38]) as well as in the range of tempered NiMn_2O_4 AD films ($\leq 10\%$ [24]). At higher aging temperatures, e.g., 200 °C (above the maximum operating temperature of 150 °C), a stronger aging occurs. Here too, the main change of B and ρ_{25} took place within the first 100 h. Above 400 °C, decomposition of the spinel is to be expected. For practical applications, processes such as pre-aging [2] or improved material compositions [5] are used. Based on these findings, miniaturized chip components were manufactured and tested.

3.2. Chip-Based NTC Thermistor Components

The following Figure 7 shows a photograph and an SEM image of the surface of the completely processed chip-based NTCR sensor devices. As already stated under Section 3.1, the combination of the substrate, the AD film and the electrode was mechanically stable without cracks, spalling or delamination. The Au electrode was precisely imaged and has the intended finger width and distance of 70 μm (Figure 7a). As shown in the SEM image in Figure 7b, the in situ calcined film structure differed from that of the aerosol deposited films [28] as well. Indeed, an AD-typical crater-like surface structure [14] could be recognized. The particles were no longer strongly deformed and no nanograined structure was evident. Instead, a recrystallized microstructure with grains in the range of 100 nm to 500 nm could be seen. As already described under Section 3.1, this structure was presumably due to the sintering process and possible sintering additives from the screen-printing paste. Nevertheless, the very dense film structure has to be emphasized. At sintering temperatures of only 850 °C, this dense film structure cannot be achieved by the classic ceramic processes due to the poor sintering properties of NTCR ceramics [17,19,39,40].

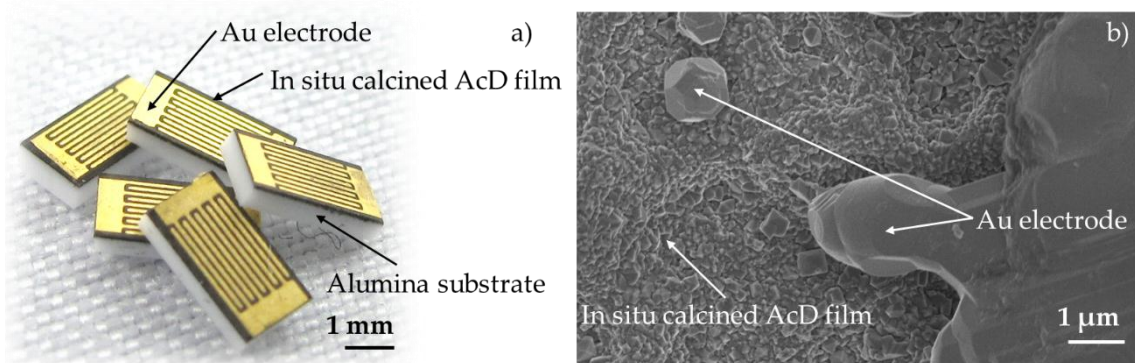


Figure 7. Finished chip-based NTCR sensor after completion of multifunctional temperature treatment (a) photograph and (b) SEM image of the surface.

So far, all sensors had been manufactured individually. Due to the miniaturized design, it is now possible to produce 50 components per deposition process. This allows statements about process noise, leading to a variation of the NTCR parameters. Figure 8 summarizes the NTCR parameters of 50 sensor components. As shown in Figure 8a, the electrical resistance of the components at 25 °C (R_{25}) was on average 65 k Ω and had a standard deviation of 4 k Ω . The R_{25} value was higher than the R_{25} value in Section 3.1, mainly because of a different electrode structure (see Section 2).

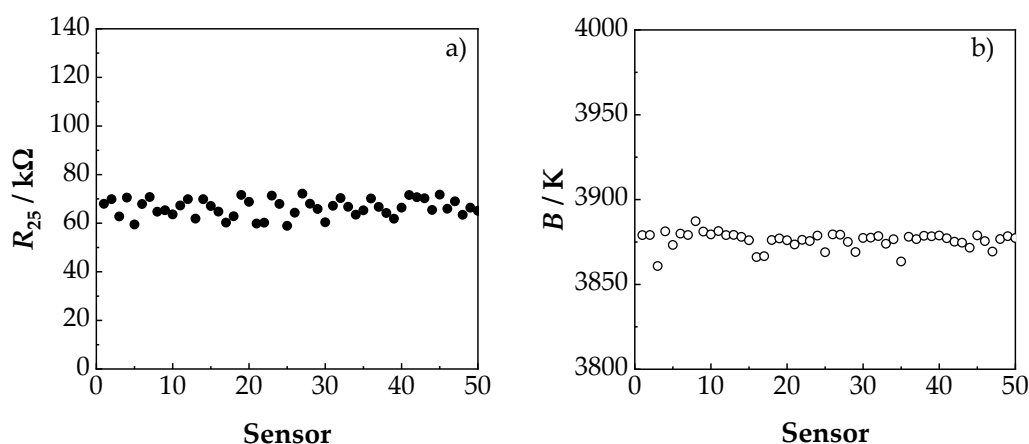


Figure 8. Determined (a) R_{25} value and (b) B values of 50 sensors.

The dispersion in the R_{25} values was due to two reasons—the homogeneity of the NTCR film thickness and the precision of the screen-printed electrode. Thus, the film thickness of the aerosol co-deposited film varied slightly, both over the nozzle width and over the film length. The same applied to the electrode structure, which also fluctuated slightly due to the manufacturing process. The B value in Figure 8b was on average 3876 K and had a standard deviation of only 5 K. The B value of 3876 K was slightly higher than the B value of 3825 K of the prototypes (Figure 5). This difference of about 1% was mainly attributed to fluctuations in the manual powder production.

Considering the aging behavior of chip-based components at 125 °C, the results (Figure 9) were similar to that of the prototypes. Here too, the R_{25} values increased by about 12% and the B values by about 1%. Thus, not only the individually prepared samples but also the industrial-like manufactured samples, showed the same aging behavior of bulk-based NiMn_2O_4 ceramics [5,38] and tempered NiMn_2O_4 AD films [24]. An increase in R_{25} of 12% was relatively high, but not uncommon for unstabilized systems such as NiMn_2O_4 [38]. An improvement could be achieved when utilizing optimized compositions as described in the literature, as in References [41–43], or when using polyphase ceramics [5,24]. For instance, Rousset et al. [5] have already observed that a polyphase ceramic of spinel and NiO reduces aging. A similar behavior could also be found with a polyphase ceramic of NiMn_2O_4 , NiMnO_3 and $\alpha\text{-Mn}_2\text{O}_3$ [24]. This polyphase ceramic ($\text{NiMn}_2\text{O}_4 + \text{NiMnO}_3 + \alpha\text{-Mn}_2\text{O}_3$) could be achieved by partial decomposition of the NiMn_2O_4 spinel by thermal post-treatment in the unstable range of >400 °C [44] to <730 °C [23].

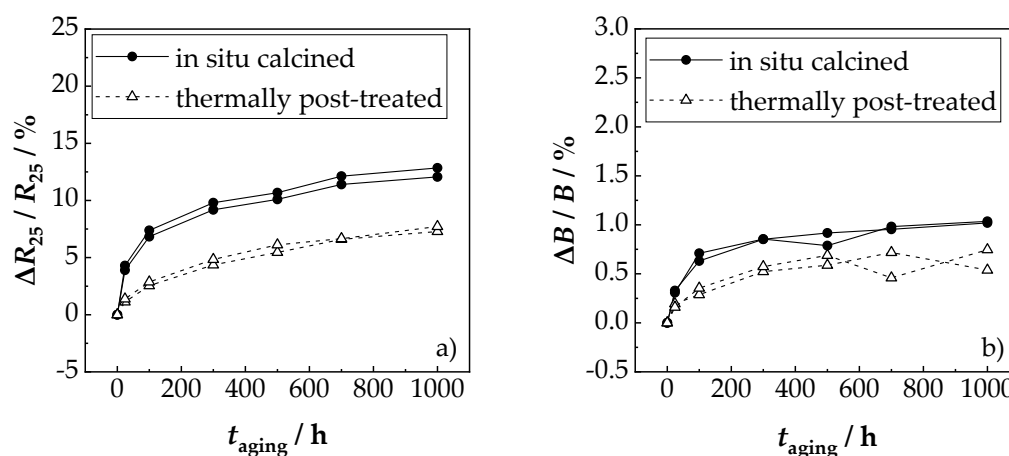


Figure 9. Aging-related change of (a) R_{25} value and (b) B value for chip-based components after 1000 h at 125 °C.

The improved aging stability is also shown in Figure 9a,b. It could be seen that subsequently, thermally post-treated components (600 °C for 60 min) were significantly less prone to aging than purely in situ calcined components. Thus, the change in the R_{25} value was only 7% and the change in the B value was only 0.6%. Consequently, an improvement in the aging stability of aerosol co-deposited films was also possible through the formation of multi-phase ceramics.

4. Conclusions

In the present study, it could be shown that on the basis of a new method, consisting of only three steps—*aerosol co-deposition of a powder mixture, screen-printing of an electrode structure, multifunctional temperature treatment*—mechanically stable NTCR sensors could be reproducibly produced. It has been shown, by means of initial prototypes, that the NTCR parameters ρ_{25} and B , as well as their aging stability, were similar to those of classic bulk NiMn_2O_4 ceramics or tempered NiMn_2O_4 AD films. Based on this novel process route, miniaturized chip-based components were developed and manufactured. These chip-based sensors exhibited the same properties as the first prototypes. It could also be shown that the components could be manufactured with high reproducibility and that aging could be improved by thermal post-treatment to form a polyphase ceramic.

Author Contributions: All authors planned the experiments. M.S. performed AcD, J.K. screen-printed the electrode structure, M.S. made the measurements and evaluated the data supervised by R.M., M.S., J.K. and R.M. wrote the manuscript. All authors discussed the results, interpreted the findings, and reviewed and revised the manuscript.

Funding: Project was funded by the Bavarian Research Foundation (Bayerische Forschungsstiftung, BFS), grant number AZ-1159-15. The publication fees were funded by the German Research Foundation (DFG) and the University of Bayreuth in the funding program “Open Access Publishing”.

Acknowledgments: We thank A. Mergner from the University of Bayreuth, Department of Functional Materials and the BPI KeyLab Electron and Optical Microscopy for the SEM images and W. Milius from the University of Bayreuth, Department of Inorganic Chemistry I (Breu) for XRD analyses.

Conflicts of Interest: The authors declare no conflict of interest.

References

1. Ma, C.; Gao, H. Preparation and characterization of single-phase NiMn_2O_4 NTC ceramics by two-step sintering method. *J. Mater. Sci. Mater. Electron.* **2017**, *28*, 6699–6703. [[CrossRef](#)]
2. Feteira, A. Negative temperature coefficient resistance (NTCR) ceramic thermistors: An industrial perspective. *J. Am. Ceram. Soc.* **2009**, *92*, 967–983. [[CrossRef](#)]
3. Csete de Györgyfalva, G.D.C.; Reaney, I.M. Decomposition of NiMn_2O_4 spinel: An NTC thermistor material. *J. Eur. Ceram. Soc.* **2001**, *21*, 2145–2148. [[CrossRef](#)]
4. Gao, H.; Ma, C.; Sun, B. Preparation and characterization of NiMn_2O_4 negative temperature coefficient ceramics by solid-state coordination reaction. *J. Mater. Sci. Mater. Electron.* **2014**, *25*, 3990–3995. [[CrossRef](#)]
5. Rousset, A.; Legros, R.; Lagrange, A. Recent progress in the fabrication of ceramic negative temperature coefficient thermistors. *J. Eur. Ceram. Soc.* **1994**, *13*, 185–195. [[CrossRef](#)]
6. Gillot, B.; Baudour, J.L.; Bouree, F.; Metz, R.; Legros, R.; Rousset, A. Ionic configuration and cation distribution in cubic nickel manganite spinels $\text{Ni}_x\text{Mn}_{3-x}\text{O}_4$ ($0.57 < x < 1$) in relation with thermal histories. *Solid State Ion.* **1992**, *58*, 155–161.
7. Darmawansyah, A. NTC thermistors sensor thick film technology. In Proceedings of the SENTIA 2009, Malang, Indonesia, 12 March 2009.
8. Schmidt, R.; Basu, A.; Brinkman, A.W. Small polaron hopping in spinel manganates. *Phys. Rev. B* **2005**, *72*, 115101. [[CrossRef](#)]
9. Fau, P.; Bonino, J.P.; Demai, J.J.; Rousset, A. Thin films of nickel manganese oxide for NTC thermistor applications. *Appl. Surf. Sci.* **1993**, *65/66*, 319–324. [[CrossRef](#)]
10. Savic, S.M.; Nikolic, M.V.; Aleksic, O.S.; Slankamenac, M.; Zivanov, M.; Nikolic, P.M. Intrinsic Resistivity of Sintered Nickel Manganite vs. Powder Activation Time and Density. *Sci. Sinter.* **2008**, *40*, 27–32. [[CrossRef](#)]

11. Reimann, T.; Töpfer, J.; Barth, S.; Bartsch, H.; Müller, J. Low-Temperature Sintered NTC Thermistor Ceramics for Thick-Film Temperature Sensors. *Int. J. Appl. Ceram. Technol.* **2013**, *10*, 428–434. [[CrossRef](#)]
12. Schaumburg, H. *Keramik: Werkstoffe und Bauelemente der Elektrotechnik*; B. G. Teubner: Stuttgart, Germany, 1994.
13. Akedo, J. Room Temperature Impact Consolidation (RTIC) of Fine Ceramic Powder by Aerosol Deposition Method and Applications to Microdevices. *J. Therm. Spray Technol.* **2008**, *17*, 181–198. [[CrossRef](#)]
14. Lee, D.-W.; Kim, H.-J.; Kim, Y.-H.; Yun, Y.-H.; Nam, S.-M. Growth Process of α -Al₂O₃ Ceramic Films on Metal Substrates Fabricated at Room Temperature by Aerosol Deposition. *J. Am. Ceram. Soc.* **2011**, *94*, 3131–3138. [[CrossRef](#)]
15. Schubert, M.; Exner, J.; Moos, R. Influence of Carrier Gas Composition on the Stress of Al₂O₃ Coatings Prepared by the Aerosol Deposition Method. *Materials* **2014**, *7*, 5633–5642. [[CrossRef](#)]
16. Johnson, S.D.; Glaser, E.R.; Cheng, S.-F.; Kub, F.J.; Eddy, C.R., Jr. Characterization of as-deposited and sintered yttrium iron garnet thick films formed by aerosol deposition. *Appl. Phys. Express* **2014**, *7*, 35501. [[CrossRef](#)]
17. Ryu, J.; Kim, K.-Y.; Choi, J.-J.; Hahn, B.-D.; Yoon, W.-H.; Lee, B.-K.; Park, D.-S.; Park, C. Highly Dense and Nanograined NiMn₂O₄ Negative Temperature coefficient Thermistor Thick Films Fabricated by Aerosol-Deposition. *J. Am. Ceram. Soc.* **2009**, *92*, 3084–3087. [[CrossRef](#)]
18. Schubert, M.; Münch, C.; Schuurman, S.; Poulain, V.; Kita, J.; Moos, R. Characterization of nickel manganite NTC thermistor films prepared by aerosol deposition at room temperature. *J. Eur. Ceram. Soc.* **2018**, *38*, 613–619. [[CrossRef](#)]
19. Schubert, M.; Kita, J.; Münch, C.; Moos, R. Analysis of the characteristics of thick-film NTC thermistor devices manufactured by screen-printing and firing technique and by room temperature aerosol deposition method (ADM). *Funct. Mater. Lett.* **2017**, *10*, 1750073. [[CrossRef](#)]
20. Baek, C.-W.; Han, G.; Hahn, B.-D.; Yoon, W.-H.; Choi, J.-J.; Park, D.-S.; Ryu, J.; Jeong, D.-Y. Fabrication and Characterization of NiMn₂O₄ NTC Thermistor Thick Films by Aerosol Deposition. *Korean J. Mater. Res.* **2011**, *21*, 42–47. [[CrossRef](#)]
21. Ryu, J.; Park, D.-S.; Schmidt, R. In-plane impedance spectroscopy in aerosol deposited NiMn₂O₄ negative temperature coefficient thermistor films. *J. Appl. Phys.* **2011**, *109*, 113722. [[CrossRef](#)]
22. Fang, D.-L.; Wang, Z.-B.; Yang, P.-h.; Liu, W.; Chen, C.-S.; Winnubst, A.J.A. Preparation of Ultra-Fine Nickel Manganite Powders and Ceramics by a Solid-State Coordination Reaction. *J. Am. Ceram. Soc.* **2006**, *89*, 230–235. [[CrossRef](#)]
23. Feltz, A.; Töpfer, J.; Schirrmeister, F. Conductivity Data and Preparation Routes for NiMn₂O₄ Thermistor Ceramics. *J. Eur. Ceram. Soc.* **1992**, *9*, 187–191. [[CrossRef](#)]
24. Schubert, M.; Münch, C.; Schuurman, S.; Poulain, V.; Kita, J.; Moos, R. Thermal Treatment of Aerosol Deposited NiMn₂O₄ NTC Thermistors for Improved Aging Stability. *Sensors* **2018**, *18*, 3982. [[CrossRef](#)]
25. Exner, J.; Fuierer, P.; Moos, R. Aerosol Codeposition of Ceramics: Mixtures of Bi₂O₃-TiO₂ and Bi₂O₃-V₂O₅. *J. Am. Ceram. Soc.* **2015**, *98*, 717–723. [[CrossRef](#)]
26. Exner, J.; Schubert, M.; Hanft, D.; Stöcker, T.; Fuierer, P.; Moos, R. Tuning of the electrical conductivity of Sr(Ti,Fe)O₃ oxygen sensing films by aerosol co-deposition with Al₂O₃. *Sens. Actuators B Chem.* **2016**, *230*, 427–433. [[CrossRef](#)]
27. Schubert, M.; Kita, J.; Münch, C.; Moos, R. Investigation of the *in situ* calcination of aerosol co-deposited NiO-Mn₂O₃ films. *Funct. Mater. Lett.* **2019**, 1950039. [[CrossRef](#)]
28. Hanft, D.; Exner, J.; Schubert, M.; Stöcker, T.; Fuierer, P.; Moos, R. An Overview of the Aerosol Deposition Method: Process Fundamentals and New Trends in Materials Applications. *J. Ceram. Sci. Technol.* **2015**, *6*, 147–182.
29. Jung, J.; Töpfer, J.; Feltz, A. Thermoanalytic characterization of NiMn₂O₄ formation. *J. Therm. Anal.* **1990**, *36*, 1505–1518. [[CrossRef](#)]
30. Exner, J.; Fuierer, P.; Moos, R. Aerosol deposition of (Cu,Ti) substituted bismuth vanadate films. *Thin Solid Films* **2014**, *573*, 185–190. [[CrossRef](#)]
31. Ryu, J.; Park, D.-S.; Hahn, B.-D.; Choi, J.-J.; Yoon, W.-H.; Kim, K.-Y.; Yun, H.-S. Photocatalytic TiO₂ thin films by aerosol-deposition: From micron-sized particles to nano-grained thin film at room temperature. *Appl. Catal. B* **2008**, *83*, 1–7. [[CrossRef](#)]
32. Kim, J.-H.; Kang, Y.-M.; Byun, M.-S.; Hwang, K.-T. Study on the chemical stability of Y-doped BaCeO_{3- δ} and BaZrO_{3- δ} films deposited by aerosol deposition. *Thin Solid Films* **2011**, *520*, 1015–1021. [[CrossRef](#)]

33. Hoshina, T.; Furuta, T.; Kigoshi, Y.; Hatta, S.; Horiuchi, N.; Takeda, H.; Tsurumi, T. Size Effect of Nanograined BaTiO₃ Ceramics Fabricated by Aerosol Deposition Method. *Jpn. J. Appl. Phys.* **2010**, *49*, 09MC02. [[CrossRef](#)]
34. Akedo, J.; Lebedev, M. Microstructure and Electrical Properties of Lead Zirconate Titanate (Pb(Zr₅₂/Ti₄₈)O₃) Thick Films Deposited by Aerosol Deposition Method. *Jpn. J. Appl. Phys.* **1999**, *38*, 5397–5401. [[CrossRef](#)]
35. Akedo, J.; Lebedev, M. Powder Preparation in Aerosol Deposition Method for Lead Zirconate Titanate Thick Films. *Jpn. J. Appl. Phys.* **2002**, *41*, 6980–6984. [[CrossRef](#)]
36. Ryu, J.; Priya, S.; Park, C.-S.; Kim, K.-Y.; Choi, J.-J.; Hahn, B.-D.; Yoon, W.-H.; Lee, B.-K.; Park, D.-S.; Park, C. Enhanced domain contribution to ferroelectric properties in freestanding thick films. *J. Appl. Phys.* **2009**, *106*, 24108. [[CrossRef](#)]
37. Rousset, A.; Tenailleau, C.; Dufour, P.; Bordeneuve, H.; Pasquet, I.; Guillemet-Fritsch, S.; Poulain, V.; Schuurman, S. Electrical Properties of Mn_{3-x}Co_xO₄ (0 ≤ x ≤ 3) Ceramics: An Interesting System for Negative Temperature Coefficient Thermistors. *Int. J. Appl. Ceram. Technol.* **2013**, *10*, 175–185. [[CrossRef](#)]
38. Metz, R. Electrical properties of N.T.C. thermistors made of manganite ceramics of general spinel structure: Mn_{3-x-x'}M_xN_{x'}O₄ (0 ≤ x + x' ≤ 1; M and N being Ni, Co or Cu). Aging phenomenon study. *J. Mater. Sci.* **2000**, *35*, 4705–4711. [[CrossRef](#)]
39. Schmidt, R.; Basu, A.; Brinkman, A.W. Production of NTCR thermistor devices based on NiMn₂O_{4+δ}. *J. Eur. Ceram. Soc.* **2004**, *24*, 1233–1236. [[CrossRef](#)]
40. Schmidt, R.; Stiegelschmitt, A.; Roosen, A.; Brinkman, A.W. Screen printing of co-precipitated NiMn₂O_{4+δ} for production of NTCR thermistors. *J. Eur. Ceram. Soc.* **2003**, *23*, 1549–1558. [[CrossRef](#)]
41. Castelan, P.; Ai, B.; Loubiere, A.; Rousset, A.; Legros, R. Aging study of nickel-copper-manganite negative temperature coefficient thermistors by thermopower measurements. *J. Appl. Phys.* **1992**, *72*, 4705–4709. [[CrossRef](#)]
42. Park, K. Improvement in electrical stability by addition of SiO₂ in (Mn_{1.2}Ni_{0.78}Co_{0.87-x}Cu_{0.15}Si_x)O₄ negative temperature coefficient thermistors. *Scr. Mater.* **2004**, *50*, 551–554. [[CrossRef](#)]
43. Cheng, F.; Wang, J.; Zhang, H.; Chang, A.; Kong, W.; Zhang, B.; Chen, L. Phase transition and electrical properties of Ni_{1-x}Zn_xMn₂O₄ (0 ≤ x ≤ 1.0) NTC ceramics. *J. Mater. Sci. Mater. Electron.* **2015**, *26*, 1374–1380. [[CrossRef](#)]
44. Tang, X.-X.; Manthiram, A.; Goodenough, J.B. NiMn₂O₄ revisited. *J. Less Common Met.* **1989**, *156*, 357–368.



© 2019 by the authors. Licensee MDPI, Basel, Switzerland. This article is an open access article distributed under the terms and conditions of the Creative Commons Attribution (CC BY) license (<http://creativecommons.org/licenses/by/4.0/>).